Mechanics and Mechanical Engineering
Vol. 22, No. 1 (2018) 239–251
© Lodz University of Technology

https://doi.org/10.2478/mme-2018-0021

Experimental Study of Flow Control Over an Ahmed Body Using Plasma Actuator

S. Shadmani
S. M. Mousavi Nainiyan
R. Ghasemiasl
Department of Mechanical Engineering
West Tehran Branch
Islamic Azad University, Tehran
Iranmousavi.mojtaba@wtiau.ac.ir

M. Mirzaei
S. G. Pouryoussefi
Department of Aerospace Engineering
K. N. Toosi University of Technology, Tehran, Iran

Received (18 September 2017)
Revised (14 October 2017)
Accepted (18 November 2017)

Ahmed Body is a standard and simplified shape of a road vehicle that's rear part has an important role in flow structure and it's drag force. In this paper flow control around the Ahmed body with the rear slant angle of 25° studied by using the plasma actuator system situated in middle of the rear slant surface. Experiments conducted in a wind tunnel in two free stream velocities of U = 10 m/s and U = 20 m/s using steady and unsteady excitations. Pressure distribution and total drag force was measured and smoke flow visualization carried out in this study. The results showed that at U = 10 m/s using plasma actuator suppress the separated flow over the rear slant slightly and be effective on pressure distribution. Also total drag force reduces in steady and unsteady excitations for 3.65% and 2.44%, respectively. At U = 20 m/s, using plasma actuator had no serious effect on the pressure distribution and total drag force.

Keywords: automotive, aerodynamics, wind tunnel, plasma actuator, Ahmed body.

1. Introduction

Increasing growth of the number of road transportation vehicles and hence fossil fuel consumption have raised air pollution level to alert status in many cities [1]. In this regard, considering international policies for reducing the consumption of fuels and greenhouse gases generated by motor vehicles, researchers in the field of car aerodynamics have tried to minimize the resisting force generated as air flow hits the vehicles. The lower amount of this force (known as drag force), the lower will be

its fuel consumption and pollutant emission [2]. This force can only be controlled by accurate characterization of the flow pattern.

Since experimental study of flow control accurately and comprehensively is an expensive and time-intensive practice due to differences in their apparent structures, and the fact that, it is not reasonable to generalize the results of such studies to other cases, it will be a useful practice to present a simple and standard model of a vehicle with similar flow pattern to that of an actual car [3]. Therefore, a model known as Ahmed body model [3] is referred to which resembles three-dimensional flow pattern of an actual car due to the rear slant angle behind that (Fig. 1).

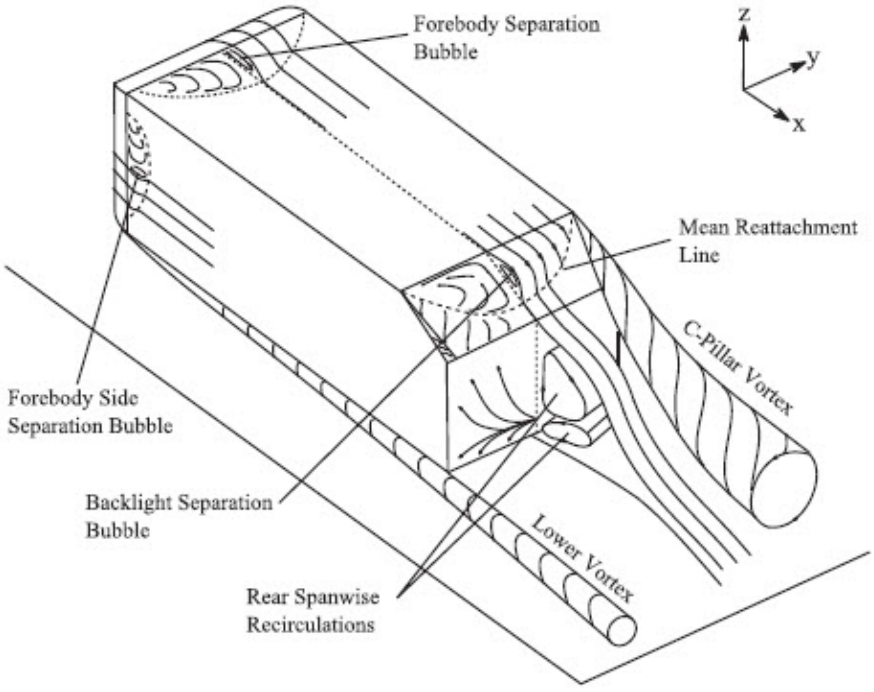

Figure 1 Flow pattern behind the Ahmed body model at rear slant angle of 25° [3]

In research works, active and passive flow controls were adopted in the tailing section of the model in an attempt to modify the flow in this region and reduce the drag force applied to the model. Installation of various types of deflectors [4, 5] is the passive flow control method which require no external energy [4]. Uncontrollable performance is a disadvantage of this method [6]. Active control methods such as mixed jets [6], pulse jets [7] and fluidic oscillators [8] are paid attention because of their controllable nature which allows them to be turned on/off on demand. Results of these methods in terms of reducing the drag force applied to Ahmed model are given in Table 1.

Table 1 Results of the research on the reduction of drag force

Drag Reduction (%)	Reynolds Number	Studies
9.3-10.7	8.7×10^5	Hanfeng et al. [4]
9	$3.1\text{-}7.7\times10^5$	Fourrie et al. [5]
6.5-8.5	1.2×10^6	Kourtaa et al. [6]
6-8	1.4×10^6	Joseph et al. [7]
7.5	1.4×10^6	Metka et al. [8]

Dielectric barrier discharge (DBD) plasma actuator is another modern tool for active flow control which is used in aviation applications. As can be observed in Figure 2, a plasma actuator is composed of two electrodes separated by a dielectric barrier, whereby air molecules above the insulated electrode is ionized by establishing a strong electric field. Known as plasma, this ionized gas extends from the edge of the upper exposed electrode to the tailing edge of the lower insulated electrode, and adds up local momentum to the flow passing above the region by colliding moving charged particles to other neutral particles of the background gas [9].

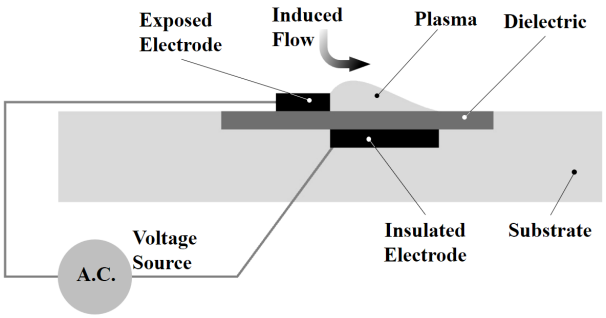

Figure 2 DBD plasma actuator mechanism

These actuators have found many applications in separation control on airfoils [10-12], and flow control on bluff bodies [13-17].

In automobile aerodynamics, Khalighi et al. 2016 [18] installed plasma actuators on the four edges of an Ahmed body at rear slant angle of 0° to analyze passing flow from the tailing part of a model and showed that drag force decreases by 21.4% at 10m/s velocity, while the reduction at 20m/s velocity is 2.8%.

In the present research, flow control around an Ahmed body is experimentally studied by using plasma actuator system that located on the middle of rear slant surface. For this aim, investigating pressure distribution, drag force and observing flow pattern was performed for the first time. Experiments carried out at Reynolds numbers of $Re = 4.5\times10^5$ and $Re = 9\times10^5$. In order to have the most complete three-dimensional flow pattern and highest drag force [3], angle of rear slant selected 25° (Fig. 3).

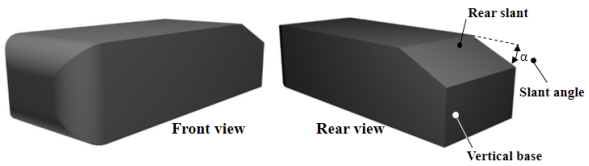

Figure 3 Plot of drag coefficient vs. slant angle (Ahmed et al. 1984)

2. Experimental details

Experiments were performed in the open circuit wind tunnel at K. N. Toosi University (Iran) with a cross sectional area of 1×1.2 m^2 and length of 3 m (Fig. 4). Turbulence intensity of the flow was below 0.2% and non-uniformity of the flow along the test section was about $\pm5\%$.

Figure 4 Used wind tunnel in this research

3. Model description

The model was constructed from 6mm-thick Plexiglas at 0.64 scale with respect to the original model. As was mentioned before, in order to establish three-dimensional flow behind the model and maximize the drag force obtained from flow separation, the rear slant angle was considered to be 25°. The model dimension was 671 × 250 × 18.5 mm^3 (length × width × height), based on which one could calculate wind tunnel section blockage ratio as 3.8%.

In order to eliminate the effects of boundary conditions on the bottom of the wind tunnel, according to Fig. 5, the model was placed on a rectangular surface at given spacing. The distance between surface and tunnel floor was 16×10^{-2}m, with the model connected to the surface via four cylindrical supports of the diameter 2×10^{-2}m and height 32×10^{-2}m. Moreover, leading edge of the surface was designed sharply to minimize the thickness of the developed boundary layer on that. Thickness of the boundary layer formed on the surface at flow velocities of 10 to 50 m/s was about 1.5×10^{-2}m [6], so that the boundary layer on the surface has no effect on the model.

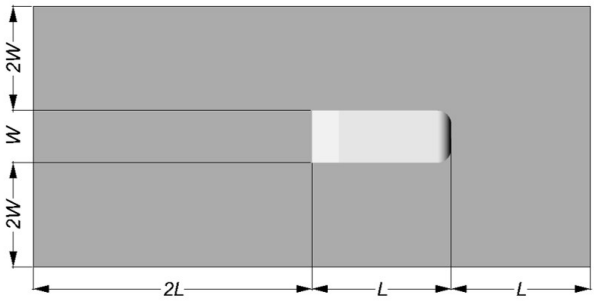

Figure 5 Position of the model on the surface

4. Instruments and measurement techniques

Pressure distribution was obtained using 52 pressure sensors (pressure transducers) installed on half of the slant and vertical surfaces of the model due to symmetry. Arrangement of the sensors is demonstrated on Fig. 6. Each sensor was composed of a tube of inner diameters of 2 mm, connected to a 28-channel pressure transducer (Honeywell-DC005NDC4). The results were monitored on a computer using an A/D (PCI6224) board, Lab view software, and Farasanjesh pressure distribution software. Sampling interval was set to 5s and pressure coefficients were calculated with the help of the Eq. 1:

$$C_p = \frac{P - P_\infty}{0.5 \times \rho \times U^2} \tag{1}$$

where P is static pressure at any point on the model, P_∞ is static pressure of free flow, U_∞ is the velocity of free flow, and ρ is air density. Uncertainty of the measurement device is about ± 0.01.

The applied drag force to the model, which is exerted to the model along the air flow, was determined using Load Cell.

Input voltage to the plasma actuator was supplied by a High-Voltage Altering Current (A.C.) with sinusoidal carrier wave and maximum output electrical power of 1000 W. Two digital multimeter sets were used to calculate actuation and carrier frequencies, with the duty cycle and applied voltage been monitored by a (GW INSTEK GDS-1072-U) oscilloscope. Furthermore, a digital multimeter (True RMS MS8226T) was used to measure mean electrical current.

According to Fig. 7, the plasma actuator position is in such a way that, the exposed and covered electrode are installed on the middle of slant, in an edge-to-edge arrangement. The electrodes were made of copper, with their thickness being 50 microns. In terms of length, the electrodes were equal to the model width 25 cm, with the widths of the open and covered electrodes being 5 and 15 mm, respectively. In all arrangements, plasma actuator dielectric was composed of six layers of Capton adhesive at breakdown voltage of 7 kV/mm and dielectric constant of 3.4.

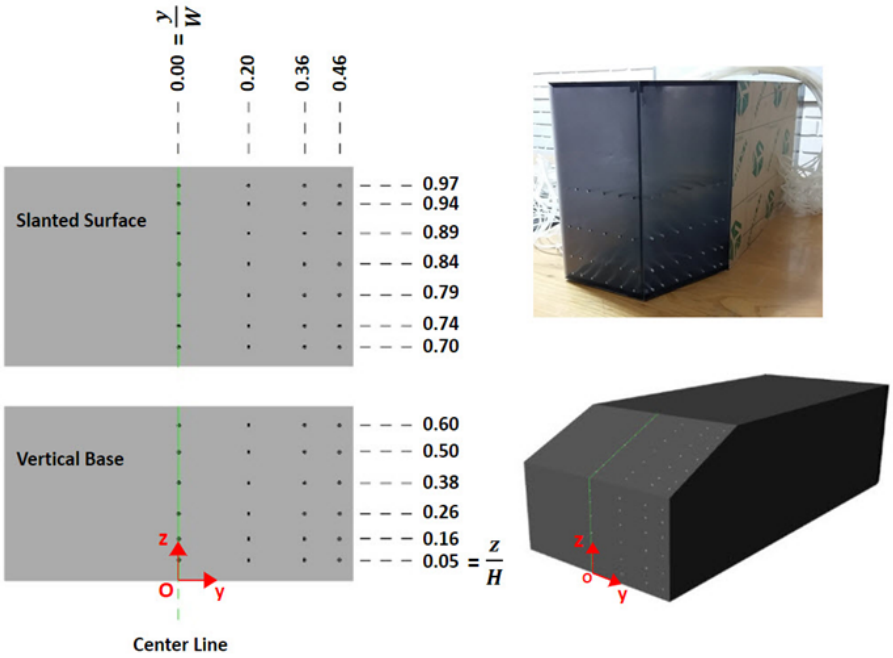

Figure 6 Position of pressure sensors

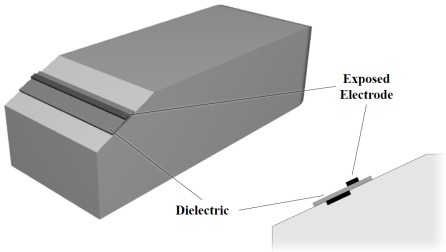

Figure 7 Position of plasma electrodes

In static flow, installing a plasma actuator on flat surface, a digital manometer (Testo 0560 5126) along with a silicon micro-tube were applied to determine maximum induced velocity based on the applied voltage, with the corresponding voltage applied in all experiments identically. In Table 2, input electrical parameters of the plasma actuator, which are used in all experiments on the model are presented.

Table 2 Input electrical parameters of plasma actuator

Duty cycle (%)	Carrier frequency (kHz)	Excitation frequency (Hz)	Voltage (kV)	Type	Velocity (m/s)	No.
100	10	-	6	Steady	10	1
50	10	20	6	Unsteady	10	2
100	10	-	6	Steady	20	3
50	10	40	6	Unsteady	20	4

5. Results and discussion

5.1. *Pressure distribution*

Three dimensional flow pattern and pressure difference between the regions in front of and behind the model develop some compressive drag force on the model. Krajnovic and Davidson [19] showed that, contribution of compressive drag force (Form drag) into total drag is about 80%. This necessitates obtaining the pattern of pressure variations across two end surfaces of the model to investigate the effect of flow across the region.

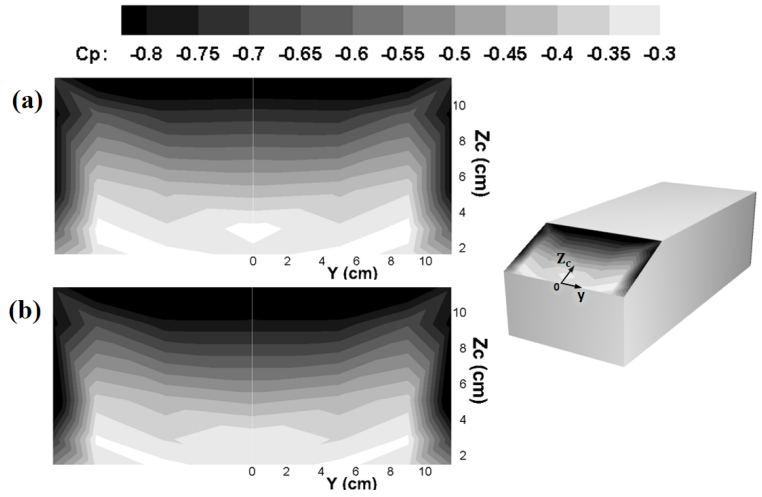

Figure 8 Contours of pressure distribution on the rear slant of an Ahmed body in plasma off mode at velocities of a) 10 m/s and b) 20 m/s

Fig. 8 shows contours of pressure coefficients distribution on the slant surface behind the model prior to the installation of the plasma actuator at U = 10 m/s (Re = 4.5×10^5) and U = 20 m/s (Re = 9×10^5), exhibiting agreement with the results reported by Joseph et al. [7], Lienhart et al. [20] and Keogh et al. 2016 [21] (Fig. 9).

According to Fig. 8, low-pressure regions of the flow extend along leading edge of the slant, so that one can stipulate that, separation bubble and flow jump over

the leading edge of slant have resulted in the development of such regions. As one moves toward central areas, the low-pressure zones are gradually replaced by zones of more pressure, i.e. the pressure is recovered. Of the other regions where low-pressure zones are developed on the surface, one may refer to lateral edges of the surface, indicating the isolation of longitudinal vortices from the top corner of the surface along the surface length (see Fig. 1).

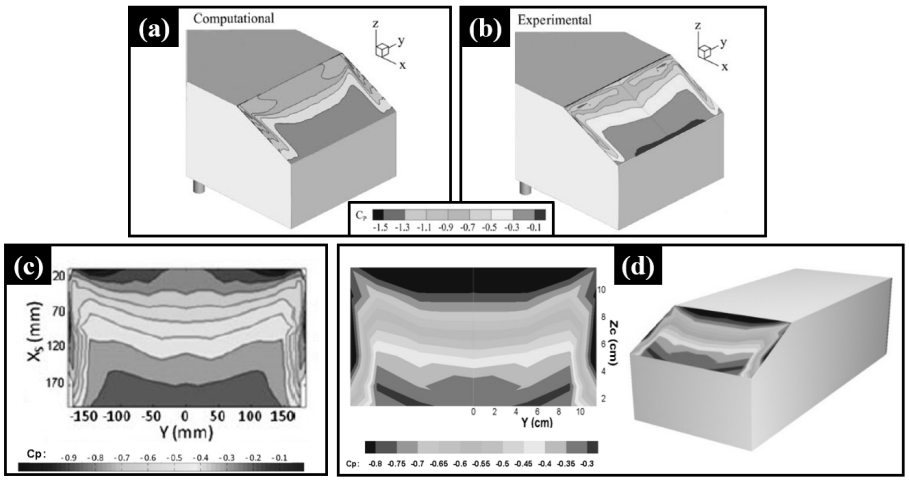

Figure 9 Contours of pressure distribution on the rear slant of the Ahmed model in velocity of 20m/s and no actuation condition in the studies of: a) Keogh et al. [21]; b) Lienhart et al. [20]; c) Joseph et al. [7] and; d) Present study

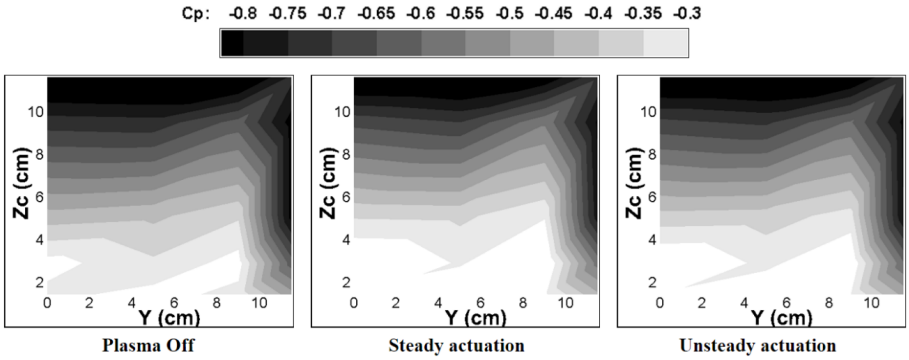

Figure 10 Contours of pressure coefficient distribution on the rear slant of Ahmed body at the velocity of 10 m/s in: a) Plasma Off, b) Steady actuation, and c) Unsteady actuation

As can be observed on Fig. 10, applying plasma actuation at the velocity of U = 10 m/s, volume of the low-pressure zones on the leading edge of the surface reduced, so that the region was much disappeared in steady state. This indicates that, actuating the plasma, the developed vortex in this zone is degraded and the separated flow tends to stick to the surface. This will be further observed in visualization tests. Moreover, a little reduction of low-pressure zones in the lateral edges of the surface is indicative of reduced effect of longitudinal vortexes behind the model. The effect of steady actuation was seen to be more significant than that of unsteady actuation. Based on Fig. 11, at the velocity of U = 20 m/s, plasma actuation imposed no significant effect on the reduction of low-pressure regions.

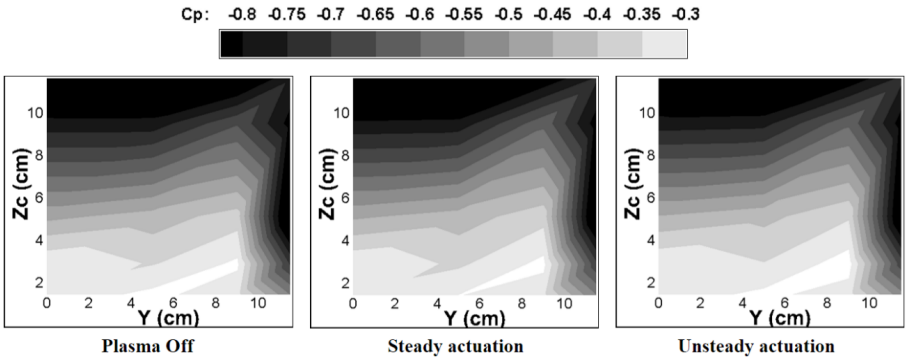

Figure 11 Contours of pressure coefficient distribution on the rear slant of Ahmed body at the velocity of 20 m/s in a) Plasma Off, b) Steady actuation, and c) Unsteady actuation

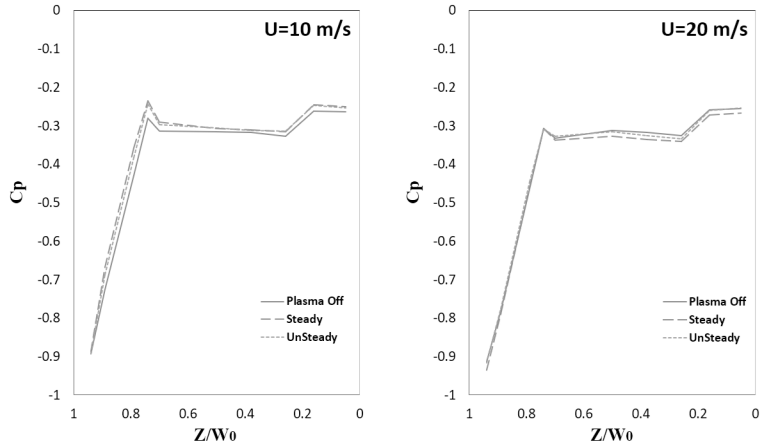

Figure 12 Plot of pressure coefficient distribution on the centerline of the model at U = 10 m/s and U = 20 m/s

Figs. 12 and 13 illustrate the plot of pressure distribution in no-actuation, steady actuation, and unsteady actuation cases on the centerline and lateral edge of the model at velocities 10 m/s and 20 m/s, respectively. Fig. 12 shows at the velocity of 10 m/s, plasma actuation increased pressure coefficients, particularly across the regions related to slant. This is while the effect of plasma actuator is insignificant at the velocity of 20 m/s. Fig. 13 indicate that at velocity of 10 m/s, plasma actuator modified and enhanced pressure coefficient diagram considerably. But as expected at velocity of 20 m/s no significant effect occurred in diagram.

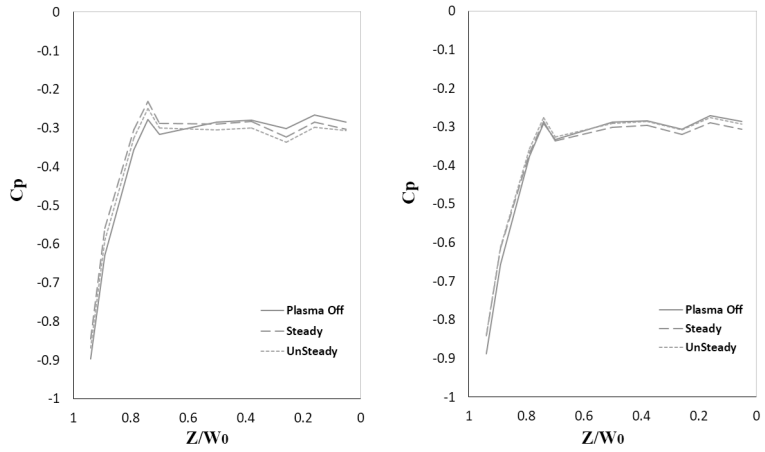

Figure 13 Plot of pressure coefficient distribution on the lateral edge of the model at velocities of U = 10 m/s and U = 20 m/s

5.2. *Drag measurement*

Total drag force applied to the model is made up of compressive and frictional drag forces applied to different regions of the model. Based on the pressure distribution pattern on the tailing surfaces of the model (described in Section 3.3), negative pressure gradient behind the model results in the formation of pressure difference between the leading and tailing zones, ending up exerting compressive drag force onto the model. The frictional force is a result of the friction and direct collision of the air flow with lateral, lower, and upper surfaces of the model. Proposing some relationships, Thacker et al. [11] specified the contribution from each of the two forces into the overall force applied to model.

In the present research, total drag force applied to the model was measured using Load cell. Prior to applying plasma actuation, the drag force applied to the model was found to be equal to 0.8 N at Re = 4.5×10^5(U=10m/s) and 3.22 N at Re = 9×10^5(U = 20m/s). Since drag force is directly proportional to the velocity squared, it can be observed that, doubling the velocity applies a force of four times as large to the model. Considering the relationship for drag force base on Eq. 2, drag coefficient of the model was found to be 0.29, which is in agreement with the

results reported in Ahmed et al. [4] (see Fig. 3).

$$C_d = \frac{F_D}{0.5 \times \rho \times A \times U^2} \tag{2}$$

where U is free flow velocity, A is effective cross-sectional area in front view, and ρ is air density in experimental conditions

Base on Fig. 14, applying plasma actuation at the velocity of 10 m/s, the values of drag force reduced by about 3.65% and 2.44% in steady and unsteady actuations, respectively. This is while, at the velocity of 20 m/s, the reduction of drag force in steady and unsteady actuations reached 0.91%. The results indicate that, at lower velocities, particularly in steady actuation, the plasma actuator can reduce overall drag force applied to the model more considerably. Considering the fact that the dominant drag force in the Ahmed model is pressure drag, the results obtained from drag force measurement using Load cell exhibit good agreement with the pressure measurement results.

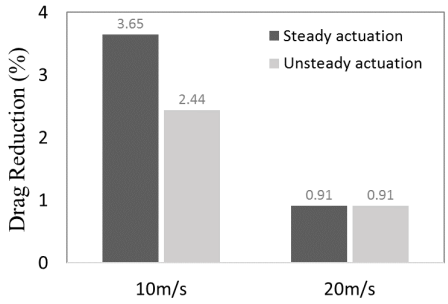

Figure 14 Plot of drag reduction

5.3. *Flow visualization*

Considering the results obtained in previous sections indicating proper performance of plasma actuator at lower velocities, in this section, the smoke flow visualization at velocity of U = 10 m/s across tailing section of the model was visualized. According to Fig. 15a, in Plasma off mode, the air flow separates from the surface as it passes over the leading edge of the rear slant, developing a vortex on the slant surface. Moreover, with the help of the flow passing through the lower part of the model, a larger vortex is formed behind the vertical surface of the model. As can be observed in Figs 15b and 15c, the plasma actuator somewhat suppresses the flow passing over the surface edge by actuating shear layer, and the separated flow from the slant surface gets closer to the surface. It is more sensible in steady actuation.

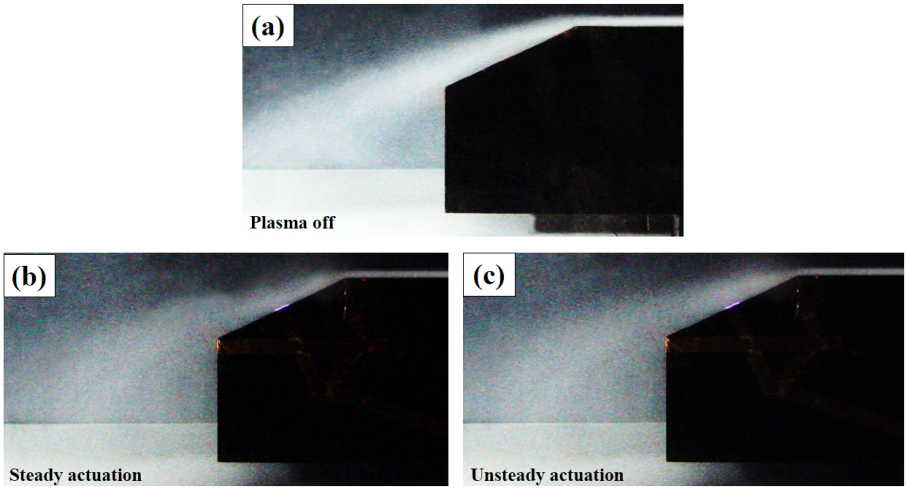

Figure 15 Pattern of the flow passing through the region behind the model at U = 10 m/s in different actuations: a) Plasma off, b) Steady actuation, and c) Unsteady actuation

6. Conclusion

In the present research, a plasma actuator was used to study flow control around an Ahmed body with a rear slant angle of 25°. Plasma actuator electrodes were installed on the middle of the rear slant surface and actuations were performed in steady and unsteady actuations at different Reynolds numbers and flow velocities of U = 10 m/s and U = 20 m/s.

Visualization results indicate that, at U = 10 m/s the plasma actuator is capable of suppressing the flow separated from the leading edge of rear slant and sticking it back to the surface by actuating the shear layer. In this case, volume of longitudinal vortexes behind the model is reduced while increasing pressure coefficient on the slant at the same time. With reducing the pressure difference between leading and tailing sections of the model, compressive drag force and hence total drag force decrease, so that the reduction of drag force in steady and unsteady actuations was 3.65% and 2.44%, respectively. At the velocity of U = 20 m/s, the results indicated that, the plasma actuator may not significantly affect pressure enhancement on ending surfaces of the model, with the reduction of drag force in both steady and unsteady state actuations being about 1%. Therefore, application of the plasma actuator at low velocities, particularly in steady actuation, can serve as an effective tool for flow control and suppression of the drag force applied to the model.

References

[1] International Energy Agency (IEA) World energy outlook 2007—China and India insights (execut. summary), *International Energy Agency*, ISBN:978-92-64-02730-5, **2007**.

[2] **Hucho, W.H.**: Aerodynamic of road vehicles, *Cambridge University Press.*, Cambridge, **1998**.

[3] **Ahmed, S.R., Ramm, G., Faitin, G.**: Some salient features of the time-averaged ground vehicle wake, *SAE Technical Paper*, No. 840300, **1984**.

[4] **Hanfeng, W., Yu, Z., Chao, Z., Xuhui, H.**: Aerodynamic drag reduction of an Ahmed body based on deflectors, *J. Wind Eng. Ind. Aerodyn*, 148, 34–44, **2016**.

[5] **Fourrie, G., Keirsbulck, L., Labraga, L., Gillieron, P.**: Bluff-body drag reduction using a deflector, *Exp Fluids*, 50, 2, **2011**, 385–395.

[6] **Kourta, A., Leclerc, C.**: Characterization of synthetic jet actuation with application to Ahmed body wake, *Sensors and Actuators A*. 192, 13–26, **2012**.

[7] **Joseph, P., Amandolese, X., Aider, J.**: Drag reduction on the 25° slant angle Ahmed reference body using pulsed jets, *Exp. Fluids*, 52, **2012**, 1169–1185.

[8] **Metka, M., Gregory, J. W.**: Drag Reduction on the 25-deg Ahmed Model Using Fluidic Oscillators, *Journal of Fluids Engineering, ASME*, 137, 051108-1, **2015**.

[9] **He, C., Corke, T.C., Patel, M.P.**: Numerical and Experimental Analysis of Plasma Flow Control Over a Hump Model, *45th Aerospace Sciences Meeting. AIAA paper*, 2007-0935, **2007**.

[10] **Post, M.L., Corke, T.C.**: Separation Control on a High Angle of Attack Airfoil Using Plasma Actuators, *AIAA Journal*, 42, 2177–2184, **2004**.

[11] **Benard, N., Braud, P., Jolibois, J.**: Airflow Reattachment Along a NACA 0015 Airfoil by Surface SDBD Actuator-Time Resolved PIV Investigation, *AIAA Paper*, 2008-4202, **2008**.

[12] **Puoryoussefi, S.G., Mirzaei, M., Alinejad, F., Puoryoussefi, S.M.**: Experimental investigation of separation bubble control on an iced airfoil using plasma actuator, *Applied Thermal Engineering*. 100, 1334-1341, **2016**.

[13] **Do, H., Kim, W., Mungal, M.O., Cappelli, M.A.**: Bluff Body Flow Separation Control Using Surface Dielectric Barrier Discharges. *AIAA Paper*, 2007-939, **2007**.

[14] **Thomas, F.O., Kozlov, A., Corke, T.C.**: Plasma Actuators for Cylinder Flow Control and Noise Reduction, *AIAA Journal*, 46, 1921-1931, **2008**.

[15] **Thomas, F.O., Kozlov, A., Corke, T.C.**: Plasma Actuators for Landing Gear Noise Control, *AIAA Paper*, 2005-3010, **2005**.

[16] **Rizzetta, D., Visbal, M.**: Large-Eddy Simulation of Plasma-Based Control Strategies for Bluff Body Flow, *AIAA Paper*, 2008-4197, **2008**.

[17] **Gregory, J., Porter, C., Sherman, D., McLaughlin, T.**: Circular Cylinder Wake Control Using Spatially Distributed Plasma Forcing, *AIAA Paper*, 2008-4198, **2008**.

[18] **Khalighi, B., Ho, J., Cooney, J., Neiswander, B., Han, T.**: Aerodynamic Drag Reduction Investigation for A Simplified Road Vehicle Using Plasma Flow Control, *Proceedings of the ASME 2016 Fluids Engineering Division Summer Meeting*, FEDSM2016-7927, **2016**.

[19] **Krajnovic, S., Davidson, L.**: Flow around a simplified car, Part 2: understanding the Flow, *J. Fluids Eng.*, 127, 919–928, **2005**.

[20] **Lienhart, H., Becker, S.**: Flow and Turbulence Structure in The Wake of a Simplified Car Model, *SAE Technical Paper*, 2003-1-0656, **2003**.

[21] **Keogh, J., Barber, T., Diasinos, S., Doig, G.**: The aerodynamic effects on a cornering Ahmed body, *J. Wind Eng. Ind. Aerodyn.*, 154, 34–46, **2016**.

[22] **Thacker, A., Aubrun, S., Leroy, A., Devinant, P.**: Effects of suppressing the 3D separation on the rear slant on the flow structures around an Ahmed body, *J. Wind Eng. Ind. Aerodyn.*, 107-108, 237–243, **2012**.